Mon. Not. R. Astron. Soc. **268,** 889–893 (1994)

The gravitational lens system B1422 + 231: dark matter, superluminal expansion and the Hubble constant

David W. Hogg and R. D. Blandford
California Institute of Technology, 130–33, Pasadena, CA 91125, USA

Accepted 1994 January 18. Received 1993 December 3; in original form 1993 July 28

ABSTRACT

A gravitational lens model of the radio quasar B1422 + 231 is presented. The model can account for the image arrangement and it can account approximately for the relative magnifications. The locations of the principal lensing mass and a more distant secondary mass concentration were predicted and subsequently luminous objects were found at these locations. This argues against the existence of substantial numbers of 'dark' galaxies. The model suggests that, if the compact radio source is intrinsically superluminal, the observed component motions may be as large as $\sim 100c$ with image B moving in the opposite direction to images A and C. The prospects for measuring the Hubble constant from a model incorporating lens galaxy locations, compact radio source expansion speeds and radio time delays, if and when these are measured, are briefly assessed.

Key words: quasars: general – quasars: individual: B1422 + 231 – dark matter – distance scale – gravitational lensing – radio continuum: galaxies.

1 INTRODUCTION

Gravitational lensing provides a direct probe of the mass distributions in astronomical objects. It is therefore important to find accurate models of lens potentials. Indeed, the existence of a compelling lens model can provide corroboration of multiple imaging. In addition, an accurate, verifiable model opens the possibility of measuring the Hubble constant if the source proves to be variable.

The B1422 + 231 system was discovered by Patnaik et al. (1992) as part of a survey of flat-spectrum radio sources. It has a redshift of $z = 3.62$, and consists of three bright components (A, B and C) and one dim component (D) all within 1.3 arcsec. There is no evidence, as yet, of extended emission. Although D is too dim for accurate spectral and polarization measurements, A, B and C have similar radio spectra and fractional polarizations. The location of D is consistent with the hypothesis that it is the fourth image of a gravitational lens system. Lawrence et al. (1992) observed B1422 + 231 in the infrared and found that all four components are in similar positions and have roughly the same flux ratios as in the radio. For these reasons, both sets of authors conclude that B1422 + 231 is a gravitational lens system.

Simple gravitational lens models of B1422 + 231 predicted a mass concentration inside the circle of images, plus a mass concentration to the south-east (Hogg & Blandford 1993). Recently, several galaxies were discovered in or near the B1422 + 231 system. Yee & Ellingson (1994) have found a galaxy (G1) inside the circle of images, and Larkin et al. (in preparation) have found two more galaxies (G2, G3) to the south-east of the quasar.

In this paper, we describe a simple lens model which provides an adequate description of existing observational data and predicts the velocity dispersions or masses of the lensing objects, the relative directions and approximate relative expansion speeds of the compact radio components (if they turn out to be intrinsically superluminal), and the relative time delays between intensity variations in the images. We find that use of the nearby galaxy locations in our model significantly improves our fits, suggesting that the recently discovered galaxies are the main contributors to the lensing potential. Future observations (e.g. with VLBI) should improve our ability to make accurate models, and thereby improve the remaining predictions.

2 OBSERVATIONS

The source B1422 + 231 was observed by Patnaik et al. (1992) with the VLA at 8.4 GHz, and with the MERLIN array at 5 GHz (Table 1). The total flux density is roughly 0.5 Jy at 5 GHz, with ~3 per cent polarization. In the optical, the combined source has the spectrum of a 16.5-mag luminous, red quasar, with absolute magnitude $M_V = -29.5 + 5 \log h$ (where h is the Hubble constant in

Table 1. Relative positions and relative 5-GHz radio fluxes of the components of B1422+231 (Patnaik et al. 1992). The coordinates θ_1 and θ_2 advance in the directions of decreasing right ascension and increasing declination, respectively, and are measured in arcseconds.

image	θ_1	θ_2	$\lvert\mu^{(iB)}\rvert$
A	-0.39 ± 0.02	0.32 ± 0.02	0.98 ± 0.02
B	0.00	0.00	1.00
C	0.33 ± 0.02	-0.75 ± 0.02	0.52 ± 0.02
D	-0.94 ± 0.03	-0.81 ± 0.03	0.020 ± 0.005

Table 2. Positions of the observed lensing galaxies G1 (Yee & Ellingson 1994), G2 and G3 (Larkin et al., in preparation), in the same coordinate system as the data in Table 1.

galaxy	θ_1	θ_2
G1	−0.70	−0.59
G2	−9.0	−5.2
G3	−3.6	−7.3

units of 100 km s^{-1} Mpc^{-1}, and $\Omega_0 = 1$). Observations by Lawrence et al. (1992) in the 2.0–2.4 μm K band, made with the Caltech 58×62 InSb array camera at the Cassegrain focus of the Hale Telescope, are consistent with the radio results.

The primary galaxy G1 was discovered by Yee & Ellingson (1994) with the CFHT. When the four known components of the B1422+231 system were subtracted, the galaxy G1 was found inside the circle of images. G2 and G3 were observed by Larkin et al. (in preparation) on a 2-μm image taken by the Keck Telescope. These two galaxies are very bright; G2 and G3 have K-band magnitudes of 16.2 and 15.7, respectively. The positions of G1, G2 and G3 are given in Table 2.

A preliminary measurement of the redshift of G1 of $z = 0.64$ was found by Hammer et al. (1993).

3 LENS MODEL

3.1 Gravitational lens theory

The lens equation relates image positions to source positions. The potential of a gravitational lens can be projected on to a two-dimensional plane (the lens plane) orthogonal to the direction of light propagation and scaled so that the lens equation is

$$\boldsymbol{\beta}(\boldsymbol{\theta}) = \boldsymbol{\theta} - \boldsymbol{\alpha}(\boldsymbol{\theta}) = \boldsymbol{\theta} - \nabla_{\boldsymbol{\theta}}\psi(\boldsymbol{\theta}), \tag{1}$$

where $\boldsymbol{\beta}$ (a two-dimensional vector) is the angular position of the source (on the source plane), $\boldsymbol{\theta}$ is that of an image point (on the image plane), $\boldsymbol{\alpha}$ is the reduced deflection, $\nabla_{\boldsymbol{\theta}}$ is the two-dimensional gradient operator with respect to $\boldsymbol{\theta}$, and $\psi(\boldsymbol{\theta})$ is the deflection potential (e.g. Schneider, Ehlers & Falco 1992; Blandford & Narayan 1992).

The inverse of the Jacobian matrix of the mapping $\boldsymbol{\beta}(\boldsymbol{\theta})$ from the image plane to the source plane is the magnification tensor $\boldsymbol{\mu}(\boldsymbol{\theta})$,

$$\boldsymbol{\mu}(\boldsymbol{\theta}) = \left(\frac{\partial\boldsymbol{\beta}}{\partial\boldsymbol{\theta}}\right)^{-1}. \tag{2}$$

The (scalar) magnification μ of an image relative to the source is the determinant of the magnification tensor.

The deflection potential ψ is related to the 'surface' mass density (mass per unit solid angle) Σ by

$$\nabla^2\psi = \frac{2\Sigma}{\Sigma_c}, \quad \text{where} \quad \Sigma_c = \frac{c^2}{4\pi G}\frac{D_d D_s}{D_{ds}} \tag{3}$$

is the critical density, and where D_d, D_s and D_{ds} are the angular diameter distances from observer to lens ('deflector'), observer to source and lens to source, respectively.

There is a time delay Δt associated with an image at $\boldsymbol{\theta}$ from a source at $\boldsymbol{\beta}$ given by

$$\Delta t = T_0\left[\frac{1}{2}|\boldsymbol{\theta}-\boldsymbol{\beta}|^2 - \psi(\boldsymbol{\theta})\right], \text{ where } T_0 = (1+z_d)\frac{D_d D_s}{c D_{ds}} \tag{4}$$

and z_d is the redshift of the lensing potential. By Fermat's principle the images are located at stationary values of $\Delta t(\boldsymbol{\theta})$ (e.g. Schneider et al. 1992).

3.2 Fitting the data

We use a general procedure to fit a gravitational lens model to the data (cf. Kayser 1990; Kochanek 1991a). In the case of B1422+231, our data comprise $n_o = 12$ observations $\{O_i\}$, namely the positions and fluxes of the four images. We suppose that these observations are normally distributed with variances σ_i^2 which we estimate from the results of Patnaik et al. (1992). We then consider lens models characterized by n_M model parameters denoted $\{M_j\}$. The number of degrees of freedom is $\nu = n_o - n_M$ (cf. Kochanek 1991b). The model parameters include lens parameters plus three more parameters which specify the location and intensity of the source on the source plane.

We seek a best-fitting solution by minimizing a least-squares figure of merit

$$\chi^2 = \sum_{i=1}^{n_o}\frac{[O_i'(\{M_j\}) - I_i]^2}{\sigma_i^2} \tag{5}$$

with respect to variation of the $\{M_j\}$, where the $O_i'(\{M_j\})$ are the values for the O_i that we derive from the model (e.g. Press et al. 1992).

Roughly speaking, a fit is good if χ^2/ν is on the order of unity. Inclusion of additional parameters in a model will almost always allow a reduction in χ^2, but this is only significant if it reduces χ^2/ν. This rule of thumb allows us to test the significance of adding additional parameters.

Prior to performing the fit, it was necessary to explore model space using the time delay surface. We identified all the extrema and then minimized a modified χ^2 obtained by deriving a source location and magnification for each image (by backwards ray-tracing), given a model, and then using the magnification tensors to convert the source displacements to

image displacements for a given source location. This is a fast procedure for searching large volumes of parameter space.

Given a particular model which minimizes χ^2, we form the Hessian matrix,

$$\mathbf{D}_{jj'} = \sum_{i=1}^{n_o} \frac{1}{\sigma_i^2} \left(\frac{\partial O_i'}{\partial M_j}\right) \left(\frac{\partial O_i'}{\partial M_{j'}}\right), \tag{6}$$

numerically, by varying the model parameters. The inverse of matrix $\mathbf{D}_{jj'}$ is the covariance matrix $\mathbf{C}_{jj'}$ which provides standard deviations for the parameters.

The goal of this model-fitting is to predict future observables, which we denote by $\{P_k\}$. In the present case, these include the relative magnification tensors of the three bright images and the time delays for variations of all four images. We compute the variances in the future observables in the usual manner:

$$\sigma_k^2 = \sum_{j,j'} \frac{\partial P_k}{\partial M_j} \mathbf{C}_{jj'} \frac{\partial P_k}{\partial M_{j'}}. \tag{7}$$

3.3 Lens potential models

The history of this project is relevant to an understanding of the results. We found first that a lens model based upon a single elliptical galaxy is insufficient to account for the large magnification ratio between images A, B and C and image D. The simplest successful lens model, which we call the initial model, comprises two singular isothermal spheres with a common redshift, each with potential $\psi = b|\boldsymbol{\theta} - \boldsymbol{\theta}_c|$, where the parameter $b = 4\pi\sigma^2 D_{ds}/c^2 D_s$, the critical radius, measures the 1D velocity dispersion σ, and $\boldsymbol{\theta}_c$ locates the centre of the potential (e.g. Kochanek 1991a; Schneider et al. 1992). (In practice, introduction of a second potential breaks the circular symmetry and avoids the structural instability of its imaging properties.) The initial model has $n_M = 9$ parameters, so $\nu = 3$.

On the basis of this model (and simple variants) we predicted that there should be a primary lensing galaxy located about one-third of the way from image D to image B, and that there should be a larger mass located about 7 arcsec south-east of image B with equivalent velocity dispersion ~ 460 km s^{-1}, presumably a small group (Hogg & Blandford 1993). Then we learned that Yee & Ellingson (1994) found the primary galaxy at the predicted location, Hanımer et al. (1993) made a preliminary measurement of the G1 redshift, and Larkin et al. (in preparation) discovered the two galaxies G2 and G3 to the south-east, near the predicted location.

Therefore we explored refined models in which we fixed the locations and redshifts of the three galaxies G1, G2 and G3 (we assume that G2 and G3 are at the same redshift as G1), and adjusted their mass distributions. We refer to the best model found in this way as the refined model. In this case, the two distant galaxies G2 and G3 are modelled as point masses, each with potential $\psi = b^2 \ln|\boldsymbol{\theta} - \boldsymbol{\theta}_c|$, where again $\boldsymbol{\theta}_c$ locates the centre of the potential, and $b^2 = M_g/\pi\Sigma_c$ measures the mass M_g of the galaxy (e.g. Kochanek 1991a; Schneider et al. 1992). Treatment of a distant galaxy as a point mass is valid if its mass distribution is roughly circular (on the sky) and none of it overlaps the circle of images. The refined model upon which we settle has $n_M = 6$, $\nu = 6$.

4 RESULTS

4.1 Lens model

The initial model is the simplest capable of approximately reproducing the observations. The centre of the primary potential is located inside the circle of images, and the secondary potential is south-east of D. The best-fitting parameters, together with the errors derived on the basis of the model, are given in Table 3. In Table 4 we give the computed magnification tensors and time delays for images A, C and D relative to image B together. The largest deficiency of this model is its failure to reproduce adequately the relative magnification of images A and B.

We experimented with several sets of adjustable parameters for the refined model. The simplest set consists of only three parameters: a velocity dispersion σ for G1, and masses M_2 and M_3 for G2 and G3. In this case, G1 is modelled as a singular isothermal sphere, and G2 and G3 are treated as point masses. This set of parameters can be expanded by adding a shear to the G1 potential, by changing the radial dependence of the G1 potential, or by fine-tuning the centre of the G1 potential within the errors of the observations of Yee & Ellingson (1994).

We found that introduction of the simple, three-parameter refined model reduced χ^2/ν from ~ 60 (for the initial model) to ~ 16. We found that addition of parameters to the refined model, such as an extra shear, a modified G1 radial dependence or a fine-tuned G1 location, did not reduce χ^2/ν any further. We settled therefore on the very simple three-parameter refined model. The best-fitting parameters for the refined model are given in Table 3; computed magnification tensors and time delays are given in Table 4. Again, the largest deficiency of the model is in reproducing the A/B magnification ratio.

The refined model has a χ^2/ν that is still quite large (~ 16), but it must be remembered that the χ^2 value depends on the uncertainties in the fluxes, which we have taken from the radio observations alone. The discrepancies between the radio and infrared observations suggest that the uncertainties in the fluxes may be higher than we have assumed. Either a reduction of about 20 per cent in the radio flux of A, or a factor of 2–3 increase in the assumed uncertainties in the A, B and C flux measurements, would be necessary to bring our best-fitting χ^2/ν values to unity. In addition, the lens model is very simple and depends upon the assumptions that the galaxies share the same redshift, and that there are no significant additional perturbations along the line of sight.

A change of the variation of mass with radius changes the time delay between the three bright images and D. For this

Table 3. Parameters for the initial and refined models with standard computed errors.

initial model		refined model	
$b^{(1)}$	0.62 ± 0.02	$b^{(G1)}$	0.75 ± 0.01
$\theta_{c1}^{(1)}$	-0.67 ± 0.03	$b^{(G2)}$	5.0 ± 0.7
$\theta_{c2}^{(1)}$	-0.60 ± 0.02	$b^{(G3)}$	1.7 ± 0.3
$b^{(2)}$	3.02 ± 0.02		
$\theta_{c1}^{(2)}$	-6.6 ± 0.4		
$\theta_{c2}^{(2)}$	-5.0 ± 0.3		

Table 4. Future observables: the computed magnification tensors $\boldsymbol{\mu}^{(iB)}$ (and magnifications $\mu^{(iB)}$) relative to image B, and time delays $\Delta t^{(iB)}$ in days after B, adopting the fiducial value $T_0 = 62\ h^{-1}$ d (arcsec)$^{-2}$.

observable	initial model	refined model
$[\boldsymbol{\mu}^{(AB)}]$	$\begin{bmatrix} 3.2 & 3.5 \\ -0.81 & -1.1 \end{bmatrix}$	$\begin{bmatrix} 2.89 & 3.18 \\ -0.88 & -1.23 \end{bmatrix}$
$[\boldsymbol{\mu}^{(CB)}]$	$\begin{bmatrix} 0.27 & 0.32 \\ 4.0 & 2.9 \end{bmatrix}$	$\begin{bmatrix} 0.34 & 0.37 \\ 3.57 & 2.62 \end{bmatrix}$
$[\boldsymbol{\mu}^{(DB)}]$	$\begin{bmatrix} 0.65 & 0.53 \\ 0.38 & 0.37 \end{bmatrix}$	$\begin{bmatrix} 0.64 & 0.53 \\ 0.33 & 0.32 \end{bmatrix}$
$\mu^{(AB)}$	−0.7	−0.77
$\mu^{(CB)}$	−0.5	−0.42
$\mu^{(DB)}$	0.04	0.03
$\Delta t^{(AB)}$	$-0.2h^{-1}$	$-0.16h^{-1} \pm 0.04$
$\Delta t^{(CB)}$	$-5h^{-1}$	$-1.0h^{-1} \pm 0.1$
$\Delta t^{(DB)}$	$+18h^{-1}$	$+29.9h^{-1} \pm 0.8$

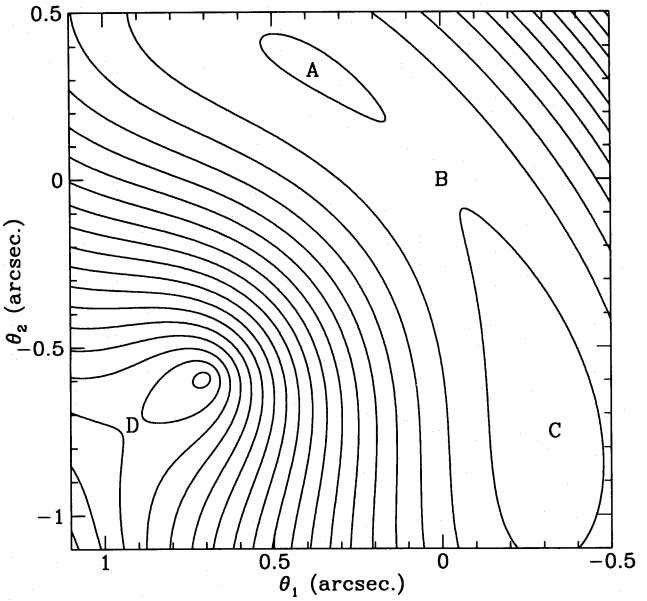

Figure 1. Time delay surface for the refined model. The images are located at A, B, C and D, and elongated along the same directions as the contours. Contours are separated by about 1.1 h^{-1} d.

reason, we believe that the B–D time delay is more uncertain than Table 4 suggests, although more simulations are necessary to verify this assertion.

(The ambitious reader may notice that our model produces two spurious images near the centres of G2 and G3. These images are only artefacts of our treatment of G2 and G3 as point masses, an approximation valid only far from the centres of G2 and G3. In fact, the actual mass distributions of G2 and G3 are spread out so that they do not exceed the critical density necessary to produce additional images of the quasar.)

4.2 Lens properties

In the refined model, the equivalent velocity dispersion of G1 is 210 km s^{-1} and the mass within the critical radius is $9.3 \times 10^{10}\ h^{-1}\ M_\odot$, consistent with a single normal galaxy. Galaxies G2 and G3 have masses of $4.1 \times 10^{12}\ h^{-1}\ M_\odot$ and $4.7 \times 10^{11}\ h^{-1}\ M_\odot$, respectively. These numbers were calculated assuming $\Omega_0 = 1$ and $z_d = 0.64$. If the redshift is significantly smaller than 0.64, the masses of G2 and G3 need not be as large to produce the same effect in the model (Browne, personal communication).

These results are consistent with the predictions of the initial model. This provides an argument against the existence of a large density of 'dark' galaxies, as gravitational lenses ought to sample all the mass in the Universe fairly.

4.3 VLBI observations

The four images of B1422+231 have a combined flux density of ~0.5 Jy. It should therefore be mappable by very long baseline interferometry (VLBI). A VLBI map that resolves the bright components will allow for more detailed models because magnification tensors, not just magnifications, may then be included in the fit.

If the source has a simple core–jet structure with superluminally moving features, then it should be possible to test the hypothesis that the core is stationary. Furthermore, the strong derived tangential (i.e. along the A–B–C arc) magnification in our models almost guarantees that the observed motion in the three bright images will also be tangential (with B's motion reversed). The absolute expansion speeds depend upon the unknown intrinsic value, but could exceed ~100c or ~9 mas yr^{-1}.

4.4 Time delay

If additional information can be obtained from radio observations, then it will remove some of the uncertainty in the shape of the time delay surface and allow a moderately accurate prediction of the relative time delay of images A and C with respect to image B, now anticipated to be several hours. (That image B's variation should follow that of images A and C and precede that of image D is mandated by the topology of the arrival time surface.) It is possible that such short delays can be measured if the source is an intraday variable (e.g. Quirrenbach et al. 1991). In this case, it will be possible to fix the multiplicative constant T_0 in the time delay and make a measurement of the Hubble constant. It may be easier to measure the time delay between images D and B. Measurement of relative magnification tensors will also help as they will remove some of the uncertainty in the shape of the time delay surface.

Even if either of these approaches furnishes a measurement of the Hubble constant, there will still be a residual uncertainty associated with the specific choice of world model and the possibility that a large screen covers the source. For example, a change of Ω_0 to ~3, while retaining $z_d = 0.64$, increases T_0 by 25 per cent. Introduction of a cosmological constant while retaining flatness for $\Omega_0 = 0.1$ (conforming with model C of Carroll, Press & Turner 1992) increases T_0 by 12 per cent.

More speculatively, Gott, Park & Lee (1989) used the observations of Q2016+112 to exclude the possibility of an

antipode at large redshift. This argument is much stronger in the case of B1422+231 because we can exhibit a successful model and the source is known to be at a higher redshift.

5 CONCLUSIONS

In this paper, we have exhibited a simple gravitational lens model for the radio-loud quasar B1422+231, despite the unprecedented, large relative magnification of ~50. That this is possible, and that the quality of the fit improved after the three galaxies were discovered, supports Patnaik et al.'s (1992) and Lawrence et al.'s (1992) claim that this source is multiply imaged. The primary lensing galaxy G1 is located within the circle of images. The galaxies G2 and G3 act perturbatively on the image arrangement, displacing image D closer to G1 (and demagnifying its flux in the process) and having the opposite effect on the other three images. B1422+231 provides a prime example of magnification bias. At both radio and visual frequencies, the source has uncommonly large flux. The combined magnification on the basis of the refined model is $\Sigma_i|\mu^{(i)}|=29$. The source quasar is therefore only 20 mag and the a posteriori probability of its having been multiply imaged is then less striking as there is a much larger parent population.

As the source is very bright at radio wavelengths, it should be possible to obtain high-dynamic-range maps of images A, B and C. We predict that all three images are elongated along the A–B–C arc, and that the parity of image B should be opposite to the parities of images A and C. We also predict large proper motions for the components along the A–B–C arc. Detailed VLBI maps that allow measurement of the relative magnification tensors may also lead to more detailed and accurate lens models.

Our final quantitative prediction is the time delay between image variations. If B1422+231 turns out to be a strong intraday variable, then it may be possible to measure this for the three bright images. (Success in this endeavour would also provide a very clean proof that intraday variability is intrinsic to compact radio sources and is not imprinted by refractive interstellar scintillation.) Relatively large flux changes in the source will be necessary to measure the predicted delay of about 1 month in the variation of the D image. Time alone will tell if the four images of B1422+231 are formed by a simple enough potential and if the source has sufficient intrinsic variability to furnish a useful measurement of the Hubble constant.

ACKNOWLEDGMENTS

We thank Ian Browne (the referee), Erica Ellingson, Chris Kochanek, Walter Landry, James Larkin, Charles Lawrence, Gerry Neugebauer, Alok Patnaik, Tony Readhead, Peter Schneider, Tom Soifer and Howard Yee for valuable discussions and encouragement. Support under the NSF Graduate Fellowship programme and NSF grants AST 89-17765 and AST 92-23370 is gratefully acknowledged.

NOTE ADDED IN PROOF

Recent radio observations by Browne (personal communication) confirm the A/B flux ratio which our model is unable to fit. Remy et al. (1993) have observed the B1422+231 system in several optical bands. Their observations are consistent with the structure found in the radio and IR, and they also find galaxies G2 and G3. As our position for G1 was measured from a preliminary sketch provided by Yee & Ellingson, the position we use for G1 differs somewhat from the position they have published (Yee & Ellingson 1994). The difference is not significant. Kormann, Schneider & Bartelmann (in preparation) have shown that the masses of G2 and G3 can be reduced if G1 is given an ellipticity.

REFERENCES

Blandford R. D., Narayan R., 1992, ARA&A, 30, 311
Carroll S. M., Press W. H., Turner E. L., 1992, ARA&A, 30, 499
Gott J. R., Park M.-G., Lee H. M., 1989, ApJ, 338, 1
Hammer F. et al., 1993, poster presented at 31st Liège Int. Astrophys. Colloq, 'Gravitational Lenses in the Universe'.
Hogg D. W., Blandford R. D., 1993, BAAS, 25, 794
Kayser R., 1990, ApJ, 357, 309
Kochanek C. S., 1991a, ApJ, 373, 354
Kochanek C. S., 1991b, ApJ, 382, 58
Lawrence C. R., Neugebauer G., Weir N., Matthews K., Patnaik A. R., 1992, MNRAS, 259, 5P
Patnaik A. R., Browne I. W. A., Walsh D., Chaffee F. H., Foltz C. B. 1992, MNRAS, 259, 1P
Press W. H., Teukolsky S. A., Vetterling W. T., Flannery B. P., 1992, Numerical Recipes in Fortran: The Art of Scientific Computing, 2nd edn. Cambridge Univ. Press, Cambridge
Quirrenbach A. et al., 1991, ApJ, 372, L71
Remy M., Surdej J., Smette A., Claeskens J.-F., 1993, A&A, 278, L19
Schneider P., Ehlers J., Falco E. E., 1992, Gravitational Lenses. Springer-Verlag, New York
Yee H. K. C., Ellingson E., 1994, AJ, 107, 28